Electronic Supplementary Material (ESI) for RSC Advances.

Electronic Supplementary Information

Magnetically Recoverable Catalysts Based on Polyphenylenepyridyl Dendrons and Dendrimers: Control over Nanoparticle Formation and Catalytic Properties

Ekaterina Yu. Yuzik-Klimova, Nina V. Kuchkina, Svetlana A. Sorokina, Bethany Boris David Gene Morgan, Linda Zh. Nikoshvili, Nadezhda A. Lyubimova, Valentina G. Matveeva, Esther M. Sulman, Barry D. Stein, Waleed E. Mahmoud, Ahmed A. Al-Ghamdi, Athanasia Kostopoulou, Alexandros Lappas, Zinaida B. Shifrina, Lyudmila M. Bronstein

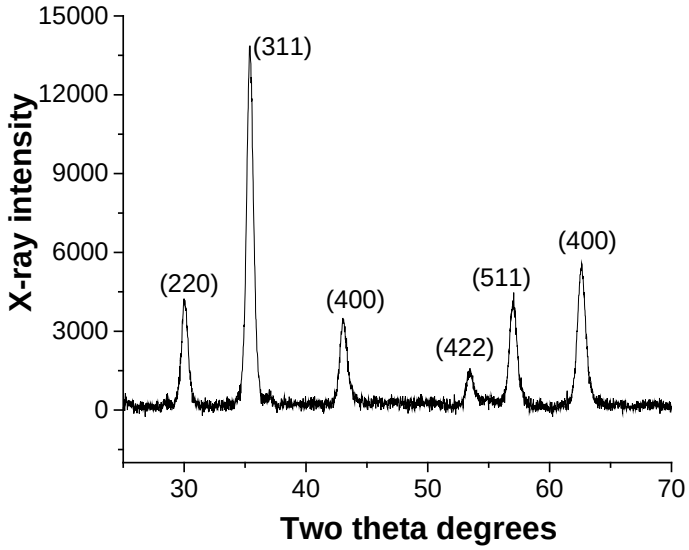

Figure S2. XRD diffraction pattern of NP**1**-1.

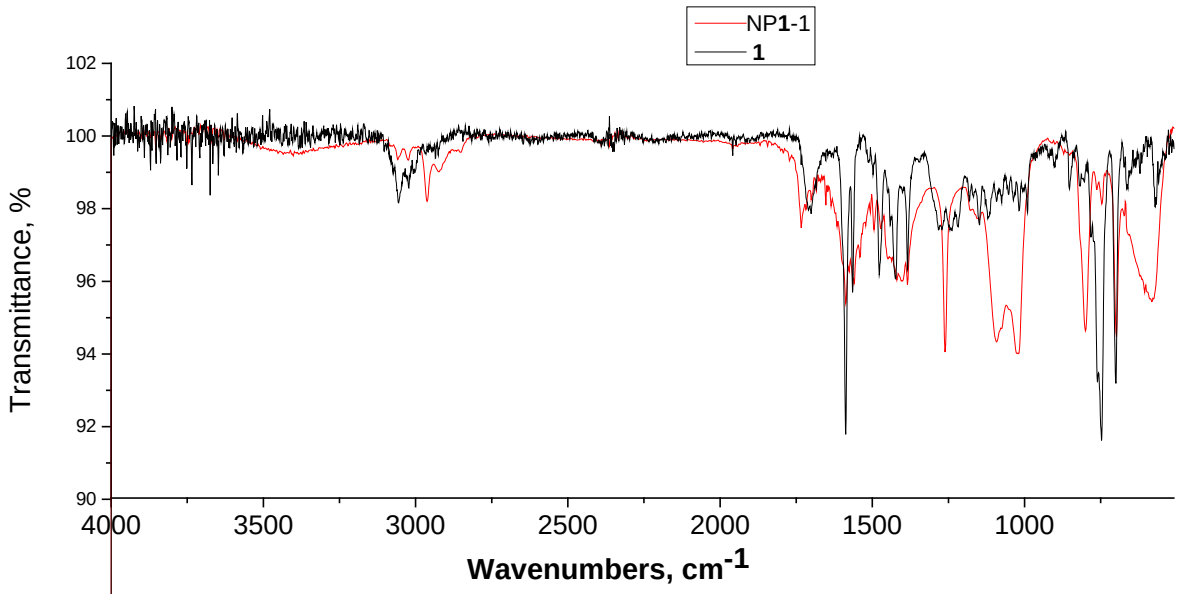

Figure S2. FTIR spectra of **1** (black) and NP**1**-1 (red).

In the FTIR spectrum of **1** (Scheme 1), two bands in the range 770-700 cm^{-1} can be assigned to out-of-plane deformation of CH. Several bands in the range 1200-950 cm^{-1} are responsible for vibrations of substituted arenes and pyridine rings. The broad bands in the range 1700-1300 cm^{-1} are the result of the bands characteristic of skeletal ring breathing modes of aromatic compounds. The weak broad bands in the range 3100-2900 cm^{-1} are due to =CH stretching modes. The very broad band at 3430 cm^{-1} is due to water around carboxyl groups. The sharp band at 1704 cm^{-1} is assigned to C=O of the carboxyl group. In the FTIR spectrum of NP**1**-1, the majority of the dendron FTIR bands become weaker or much broader because of the adsorption on the NP surface. The strong bands at 1261, 1091, 1026, and 804 cm^{-1} are associated with Fe-OH vibrations due to migration of acidic protons from capping molecules to iron oxide. The broad band at 582 cm^{-1} is assigned to the Fe-O vibrations of iron oxide.[1] The bands in the range 3100-2900 cm^{-1} associated with =CH stretching modes of arenes and pyridine rings

partially weaken and partially shift towards shorter wavenumbers indicating coordination of these rings with Fe ions.

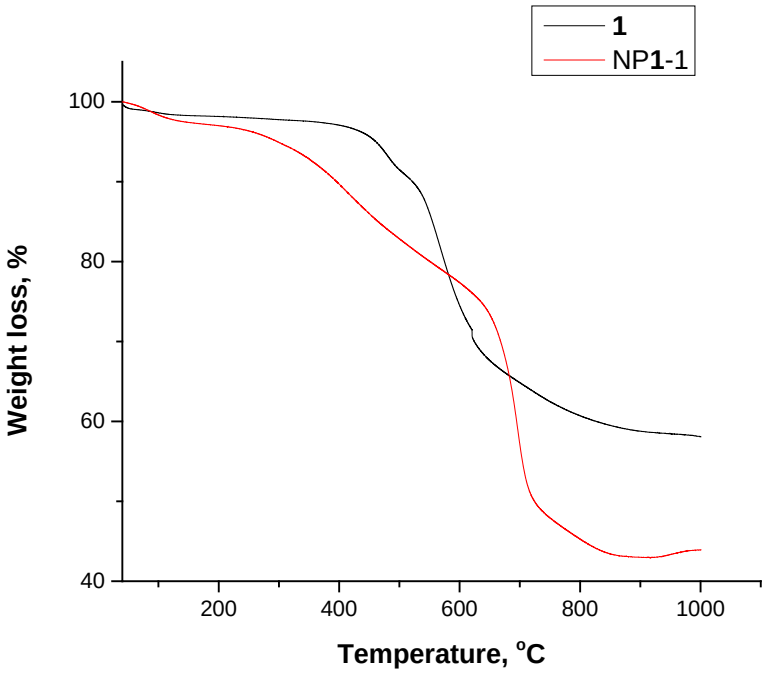

Figure S3. TGA traces of **1** (black) and NP**1**-1 (red).

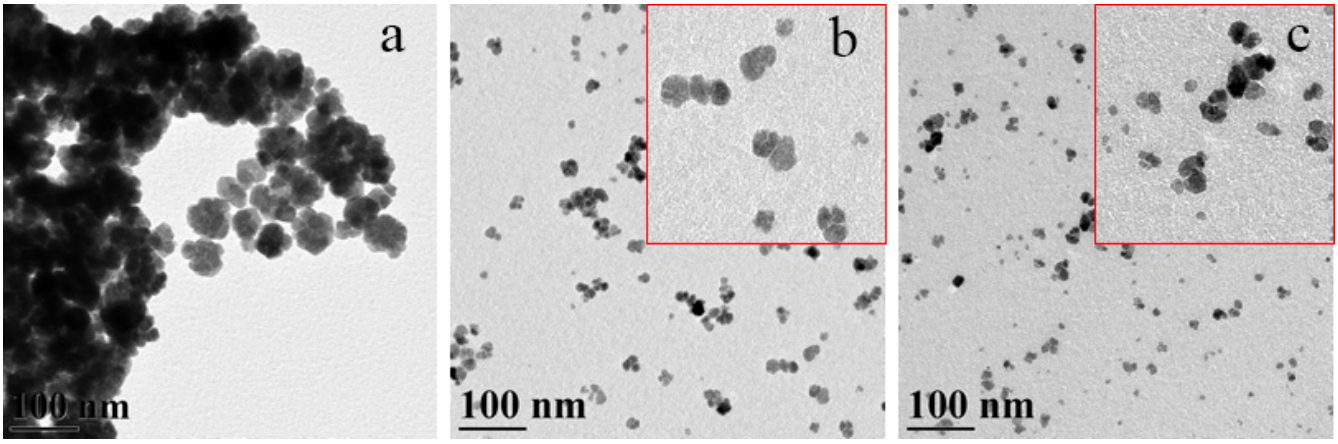

Figure S4. TEM images of NP**2**-1 (a), NP**2**-2 (b), and NP**2**-3 (c).

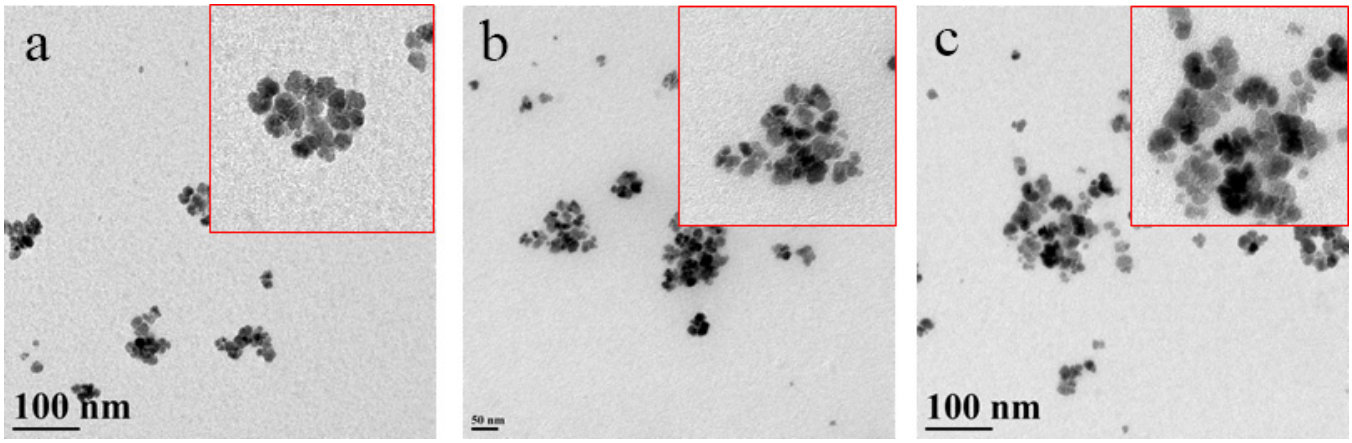

Figure S5. TEM images of NP**4**-1 at the molar ratio of Fe:**4** = 1:0.055 (a), NP**5**-1and NP**5**-2 at the molar ratios of Fe:**5** = 1:0.077 (b) and 1:0.365 (c), respectively.

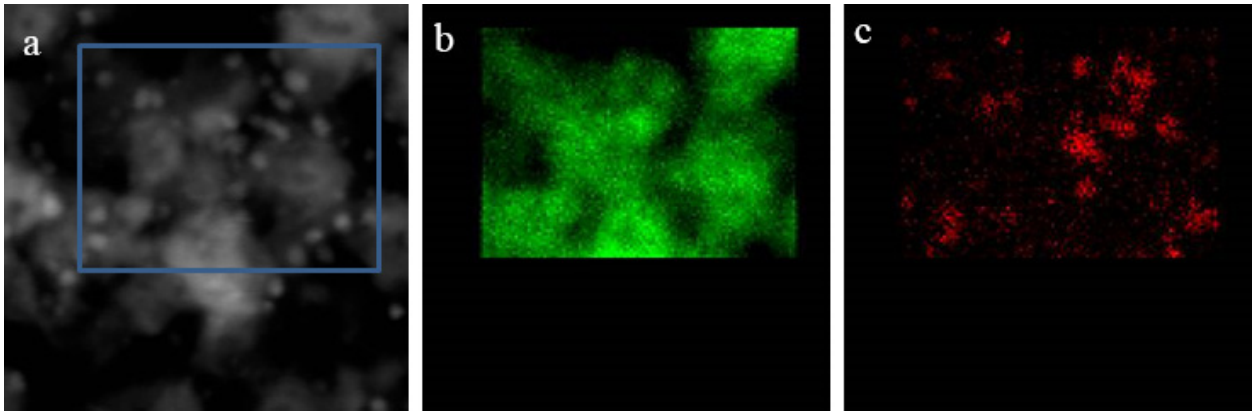

Figure S6. Dark-field STEM image (a) and EDS Fe (b) and Pd (c) maps of the NP**1**-1-PdNP sample

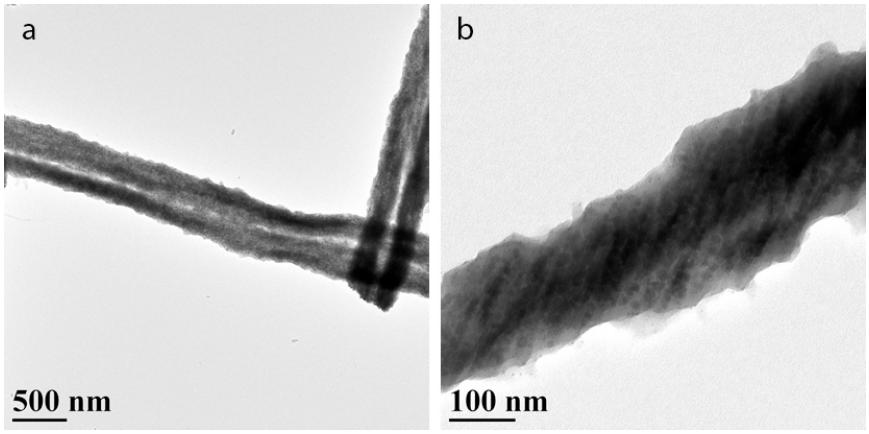

Figure S7. TEM images of NP**2**-1-PdNP at lower (a) and higher (b) magnifications.

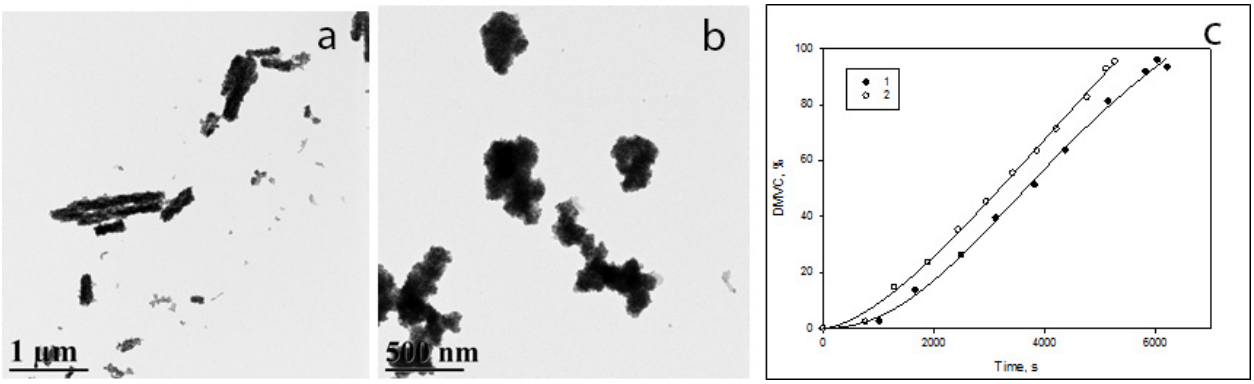

Figure S8. TEM images of NP**1**-1-PdNP-I (a) and NP**1**-1-PdNP-II (b) obtained with slow and fast addition of Pd acetate, respectively, and kinetic curves of the DMVC accumulation with those catalysts (1 and 2, respectively).

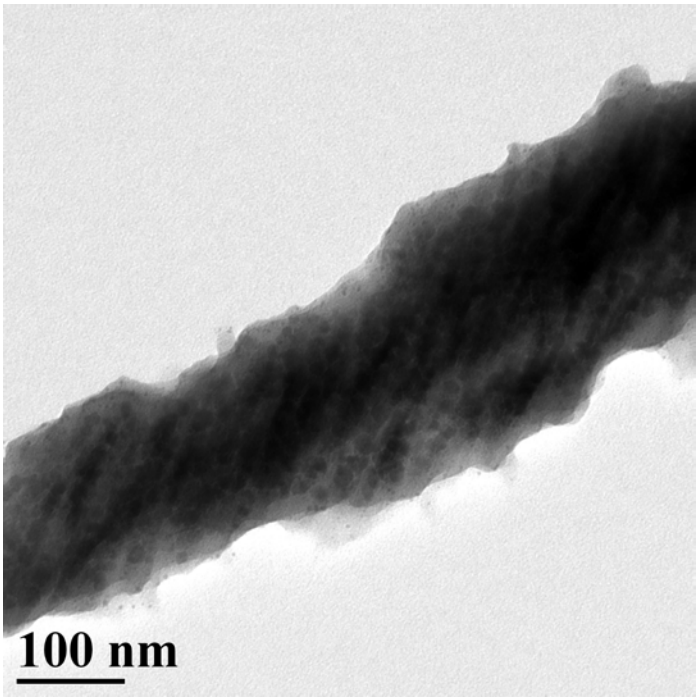

Figure S9. TEM image of NP**3**-1-PdNP.

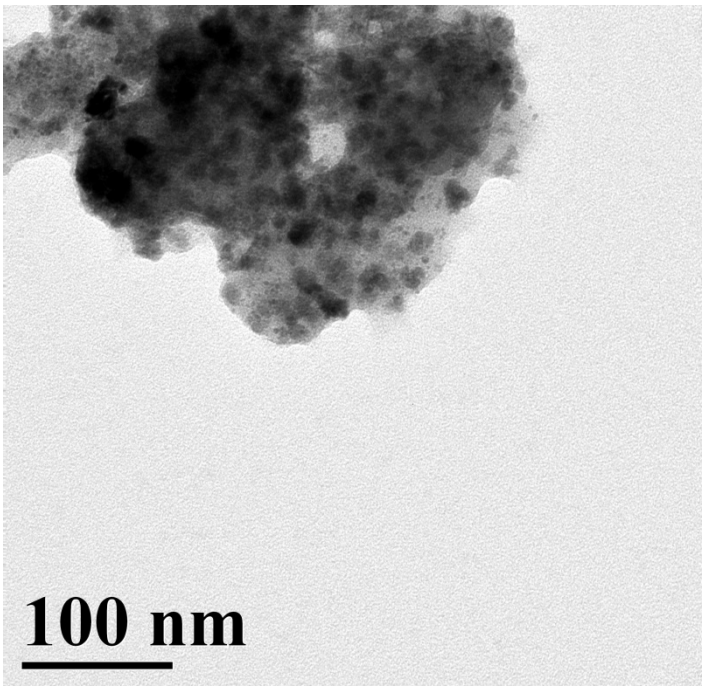

Figure S10. TEM image of NP**4**-1-PdNP after pretreatment with hydrogen before hydrogenation.

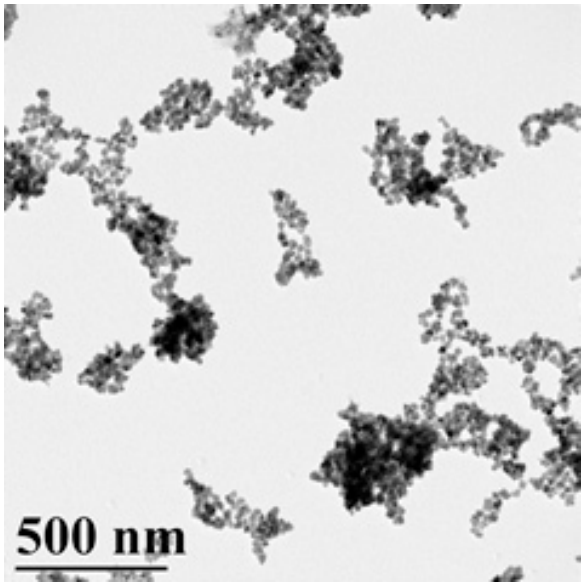

Figure S11. TEM image of the NP**4**-1 after interaction with Pd acetate.

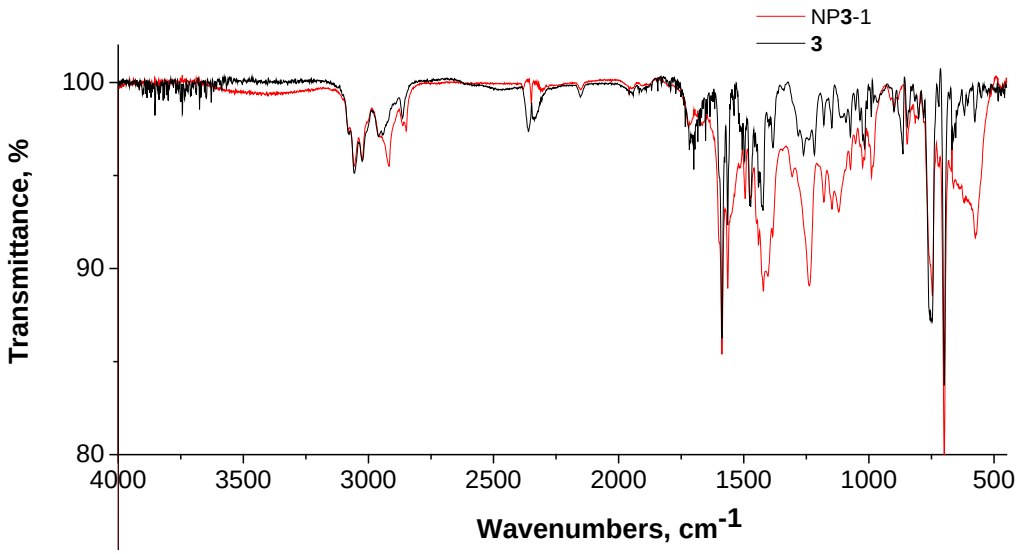

Figure S12. FTIR spectra of **3** (black) and NP**3**-1 (red).

References

(1) Hong, R. Y.; Pan, T. T.; Han, Y. P.; Li, H. Z.; Ding, J.; Han, S. *J. Magn. Magn. Mater.* **2006**, *310*, 37.